Petrographic analysis and palaeoenvironmental reconstruction of density flow deposits in the Orbuklukeli section, Mersin Mélange, Southern Turkey

Noah Lindqvist Lindström

Dissertations in Geology at Lund University,
Bachelor's thesis, no 737
(15 hp/ECTS credits)

Department of Geology
Lund University
2026

Petrographic analysis and palaeoenvironmental reconstruction of density flow deposits in the Orbuklukeli section, Mersin Mélange, Southern Turkey

Bachelor's thesis
Noah Lindqvist Lindström

Department of Geology
Lund University
2026

Table of Contents

Cover Picture: Orbuklukeli section in Turkey. Photo: Niklas Gunnarsson

Petrographic analysis and palaeoenvironmental reconstruction of density flow deposits in the Orbuklukeli section, Mersin Mélange, Southern Turkey

Noah Lindqvist Lindström

Lindström Lindqvist, Noah. 2026: Petrographic analysis and palaeoenvironmental reconstruction of density flow deposits in the Orbuklukeli section, Mersin Mélange, Southern Turkey. *Dissertations in Geology at Lund University*, No. 737, 22 pp. 15 hp (15 ECTS credits).

Abstract: During the late Triassic period several global environmental changes took place, including climate instability, and the most distinctive one was the biotic extinction at the Norian – Rhaetian boundary (NRB). Large carbonate platforms were established along the Tethys ocean and periodically exported carbonate sediments to the adjacent ocean floor, and especially at the bathyal depth.

Petrographic analysis of eleven samples from six density flow deposits in the Orbuklukeli-section in the Tavuscayiri-block, Mersin Mélange, southern Turkey, was carried out to interpret their local source area and transport mechanisms. The results of petrographic and carbonate microfacies analysis indicate that the recurrent density flow deposits were sourced from different environments. The lowermost (oldest) density flow (DF1) is interpreted to originate from a shallow water environment with indicators of the green algae order Dasycladales and early botryoidal cement. There is also an alternative interpretation for density flow 1 which interpret a hydrothermal seamount-collapse, which is supported by organic matter found in SEM-analysis. Density flows 2 – 6 are interpreted to mainly originate from slope to outer shelf environments where indicators like bivalve filaments, crinoids, calcispheres and tubiphytes support this interpretation**.**

Keywords: Petrographic analysis, Density flow deposits, Carbonate microfacies, Late Triassic, Norian-Rhaetian boundary, Mersin Mélange, Paleoenvironmental reconstruction.

Supervisor(s): Sylvain Richoz, Niklas Gunnarsson

Subject: Petrographic Geology

Noah Lindqvist Lindström, Department of Geology, Lund University, Sölvegatan 12, SE-223 62 Lund, Sweden. E-mail: noah.edvin.anton@gmail.com

Petrografisk analys och paleomiljörekonstruktion av density flow-avlagringar I Orbuklukeli-sektionen, Mersin Mélanget, södra Turkiet.

Noah Lindqvist Lindström

Lindström Lindqvist, Noah. 2026: Petrografisk analys och paleomiljörekonstruktion av density flow-avlagringar I Orbuklukeli-sektionen, Mersin Mélanget, södra Turkiet. *Examensarbeten i geologi vid Lunds universitet*, Nr. 737, 22 sid. 15 hp.

Sammanfattning: Under sen Trias inträffade flera globala miljöförändrigar, inclusive klimatinstabilitet, och den mest markanta var det biotiska utdöendet vid Norian-Rhaetian-gränsen (NRB). Stora karbonatplattformar etablerades längs tethyshavet och exporterade periodvis karbonat-sediment till det angränsade havsbottnet, särskilt på bathyalt djup.

Petrografisk analys av elva prover från sex density flow-avlagringar i Orbuklukeli-sektionen i Tavuscayiri-blocket, Mersin Mélanget, södra Turkiet, genomfördes för att tolka deras lokala källområde och transportmekanismer. Resultaten av den petrografiska och karbonat-mikrofacies-analysen indikerar att de återkommande density flow-avsättningarna härstammar från miljöer. Det understa (äldsta) density flow 1 (DF1) tolkas ha sitt ursprung i en grundvattenmiljö med indikatorer som den gröna algen *Dasycladales* och tidigt botryoidal cement. Det finns även en alternativ tolkning för density flow 1 som föreslår en hydrotermal seamount-kollaps, vilket stöds av organiskt material identifierat i SEM-analysen. Density flow 2-6 tolkas huvudsakligen ha sitt ursprung i slope– till yttre hyllmiljöer, där indikatorer som bivalvfilament, crinoider, calcisfärer och *Tubiphytes* stöder denna tolkning.

Nyckelord: Petrografisk analys, Density flow-avlagringar, Karbonatmikrofacies, Sen Trias, Norian-Rhaetian-gränsen, Mersin Mélange, Paleomiljörekonstruktion.

Handledare: Sylvain Richoz, Niklas Gunnarsson

Ämnesinriktning: Berggrundsgeologi

Noah Lindqvist Lindström, Geologiska institutionen, Lunds universitet, Sölvegatan 12, 223 62 Lund, Sverige. E-post: noah.edvin.anton@gmail.com

1 Introduction
This is the body text which uses the Style ”Body Text” (TNR10). The should be no identation at the first sentence of a new chapter, and no empty row between the title and the first sentence.

This is the second paragraph. It also uses the Style ”Body Text” but you have to indent the first line with the TAB-key.

While adding text it should flow over to the text boxes on the following pages. As you continue to add more pages you may have to link the text boxes to make the text flow through the pages.

Late Triassic was a period with several significant environmental changes, among them the Norian – Rhaetian boundary (NRB) extinction (Rigo et al., 2020). The Tethys Ocean was an important sedimentary basin during this period through large carbonate platforms which produced large volume of carbonate sediments which periodically redeposited de eper on the ocean floor (Preto et al., 2010; Reijmer et al., 2012). The NRB is dated to be around 208.5 Ma and is remarkable for its environmental disturbance and decline of biodiversity (Galbrun et al., 2020).

This study uses samples from the Orbuklukeli section in the Tavuscayiri-block of the Mersin Mélange in southern Türkiye (Tekin et al., 2020; Tekin et al., 2018). The studied section mainly constitutes alternating chert and pelagic limestone. Thi s succession is interrupted by recurrent density flow deposits, which are the focus for this study. The density flows of the Tavuscayiri-block have not been studied in detail previously, and this study aims to investigate their petrography to determine their composition and source area. Indeed, the traditional depositional settings of density flow deposits are at odds with the general deep pelagic setting represented by the enclosing sediments. The Orbuklukeli is a promising section to further understand the little documented NRB extinction. To understand the significance of the density flow deposits may help to get a better un derstanding of the environmental settings of the section and the environmental disturbances recorded there.

A density flow is a type of sedimentary gravity flow where grain-to-grain interactions are the dominating mechanism for particle-support and where the sediments are transported with gravity downslope (Mulder & Alexander, 2001). Mechanisms that can contribute to initiation of density flows include earthquakes, oversteepening of slopes and differential compaction (Flügel, 2010).

2 Background
The last stages of the supercontinent of Pangea persisted during Norian and Rhaetian stages of late Triassic (~201-227 Ma) (Ogg et al., 2020). The Tethys Ocean developed through large scale tectonic extension and was opening the supercontinent as an embayment from the east which divided the supercontinent into the landmasses in north (Laurasia) and south (Gondwana) which is depicted in the paleogeographic map on figure 1. (Preto et al., 2010). During the late Triassic, Turkey was located on the northern margin of Gondwana, i.e. southern margin of

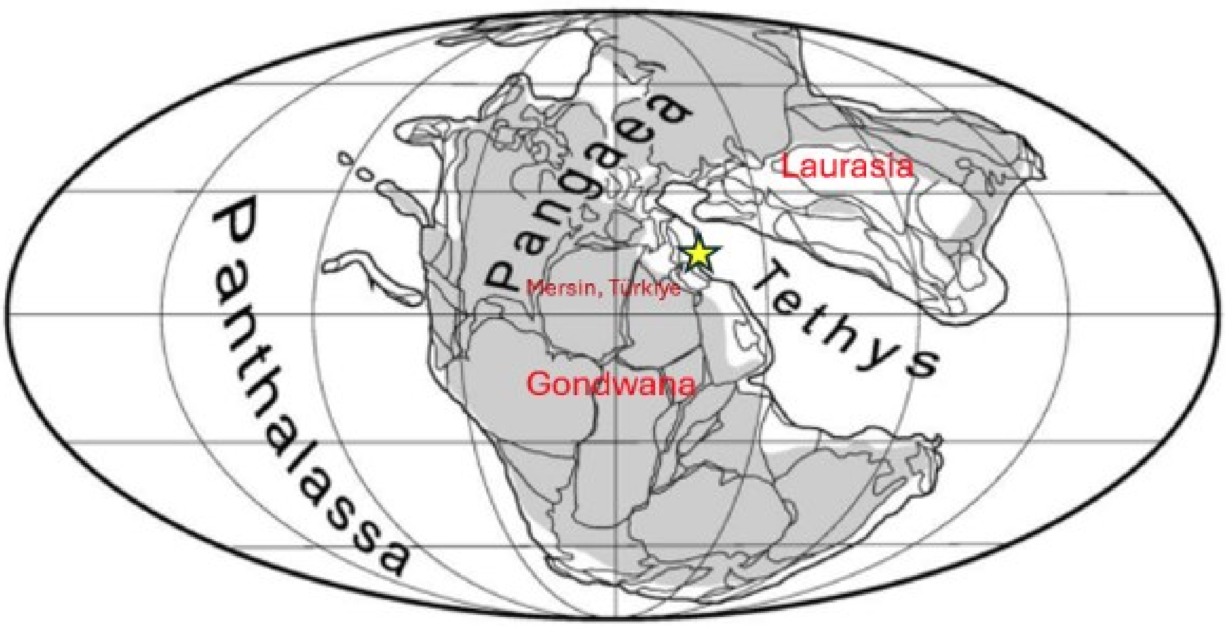

Figure 1. Map of Pangea during the Triassic period with the study area marked with a star. (figure modified from Preto et al (2010))

the Neotethys (Tekin et al., 2020).

A global "mega-monsoon" dominated the weather during the Triassic with heavy seasonal rainfall that dominated the Eastern Pangea (Preto et al., 2010). The west of Tethys Ocean where modern-day Turkey was situated, had strong alternating season al climate with dry periods and wet periods dominated by monsoon (Preto et al., 2010). In contrast to the rest of the Triassic, the Norian and Rhaetian are considered as long periods of climati c stability (Ogg et al., 2020). At the end of the Rhaetian, the volcanic activity associated with the Central Atlantic Magmatic Province (CAMP) induced an increase of greenhouse gases, which increased the temperatures, the evaporation; the humidity intensified, which contributed to increased continental weathering rates (Rigo et al., 2024; Rigo et al., 2020).

2.1 Norian-Rhaetian boundary (NRB)

The NRB is dated at 208.5 Ma and is known for its association with pronounced environmental changes and a decline in marine biodiversity (Maron et al., 2015; Rigo et al., 2020). The biodiversity decline is recognized as the "NRB-extinction", which preceded the end-Triassic mass extinction (Rigo et al., 2020). Some researchers argue that the NRB is identified geochemically by a negative carbon isotope excursion, which indicates a global interruption of the carbon cycle (Rigo et al., 2024; Rigo et al., 2020). Large changes in strontium-, osmium-, and calcium isotopes in the ocean reflect that substantial environmental changes were at play, but these are still not well understood (Kovács et al., 2022; Kovács et al., 2020; Rigo et al., 2024).

Figure 2. The Orbukukeli hill with an arrow showing what is stratigraphic up and stratigraphic range of the succession exposing density flow deposits1 to 6. White lines display density flow 2.

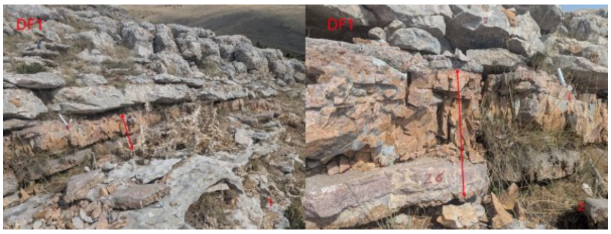

Figure 3. Field photograph of Density flow 1 (DF1). A: Overview photograph with an arrow depicting the thickness of DF1 with alternating pelagic limestone and chert above and below. Close-up with an arrow depicting the thickness of DF1.

Figure 4. Density flows (DF2-DF6) in field and arrows depicting the thickness of density flows.
1: Density flow 2 is a conglomerate with no clear way up in structure. 2: Density flow 3 is a horizontal orthoconglomerate bed with no internal bedding. 3: Density flow 4 is a conglomeratic limestone with three internal horizontal beds. 4: Density flow 5 is a bed of beige-colored limestone. 5: Density flow 6 is an Orthoconglomerate (gravel sized, clasts supported) with limestone clasts in a calci-mudstone matrix.

2.2 Geological setting

The studied succession outcrops at the locality Orbuklukeli, southern Turkey (36°55'17"N, 34°13'30"E). The section is part of the Tavuscayiri-block, a block inside the larger-scale tectonostratigraphic Mersin Mélange (Parlak & Robertson, 2004; Tekin et al., 2020). The Mersin Mélange is a part of a bigger complex called Mersin Ophiolitic Complex. The Mersin Ophiolitic Complex outcrops in a 15 km wide and 40 km long southwards area (Parlak & Robertson, 2004). The Mersin Mélange consists of Upper Triassic ophiolite intermingled with density flow units, pelagic carbonates, radiolarian chert and deformed olistolithe of different oceanic and continental origins (Parlak & Robertson, 2004). The studied section represents its bathyal part, which consists of alternating limestone-chert and intercalated density flows.

The Tavuscayiri-block is the largest and best exposed block of the central Mersin Mélange and preserves a continuous sequence of pelagic sediments that range in age from the Norian to the Toarcian (Tekin et al., 2020). The studied section at the Orbuklukeli Hill consists of a 170 m thick section of alternating limestone-chert beds with intercalated density flow deposits. The depositional environment was the bathyal, with depths of around 200 – 2000 meters (Gallet et al., 2007; Tekin et al., 2020). The Norian-Rhaetian boundary was previously identified and constrained through conodont biostratigraphy (L. Krystyn, as cited in N. Gunnarsson, personal communication, March 25, 2026).

In the studied section, there are beds with sedimentary evidence of mass movement. The beds consist of brecciated limestone-bodies which can be several meters thick and which are enclosed within limestone-chert cycles representing the background sedimentation (Tekin et al., 2020). Density flows generally occur when there is instability in the sea-floor slope which triggers the sediments to flow downwards (Reijmer et al., 2012; Tekin et al., 2020). Brecciated limestone indicates that there was a tectonically instability in the area which contributed to the density flows (Tekin et al., 2020). NRB is also interpreted as having a higher yield of seismic activity (Tekin et al., 2020).

3 Method

The samples used for this project were previously collected in Turkey by the supervisor group. Each bed was measured and sampled with a geological hammer. The samples studied are from density flows and the names for each bed sample are OR25, OR26, OR27, OR28, OR29, OR35, OR36, OR50, OR59, OR72 and OR76. The samples were contained in plastics bags until the production of thin-sections at Lund University started.

3.1 Thin-section preparation

Rock samples were cut with a rock saw and polished with sandpaper. First, we polished with either sandpaper 220 or 300; the process proceeded until the surface was even. After the surface was even, sandpaper 500 was used to get a smoother surface and after sandpaper 500 is done we proceeded to diamond-paper 500 and 1200. Next process is picking out thin-section glass and polishing it with diamond-paper 500 until the whole glass can stick epoxy to it. After polishing the glasses, these were cleaned with ethanol to erase fingerprints. The samples were stuck with epoxy to the glass and harden for two days. For samples with higher content of quartz, a second mixed solution of epoxy and acetone was added from the top to penetrate the porosity of the rock.

After the epoxy had hardened, the samples were cut as thin as possible before grinding them down until the sample was translucent.

The final process was to polish the sample until it was suitable for microscoping the bioclasts. This process starts with diamond-paper 500 until the bioclasts are clear enough, then we use diamond-paper 1200 to get a more polished surface.

3.2 Microscopy

Polarization microscopy was used for microfacies classification according to the Dunham (1962) scheme, as revised by Embry & Klovan 1971. Depositional texture as a whole was classified and Dunham terminology was also used for lithoclasts. Thereafter, I identify the bioclasts and o ther key features which are relevant for identifying the depositional environment. Any useful information is documented on an excel sheet.

3.3 SEM-analysis

The two samples OR26 and OR27 have been analyzed with Scanning Electron Microscopy (SEM). It uses electrons to depict a further enlarged (compared to microscopy using light which has 1000x as highest enlargement) picture up to 1 000 000x of a sample to get a further analysis of the samples (Ali et al., 2023).

The SEM can provide chemical compound analysis, crystal structure, and electric functions. It is also a non-damaging tool for the sample (Ali et al., 2023).

The SEM have 3 different main electron canons which are used to emit an electron beam (Ali et al., 2023):

- The Tungsten Filament which emits electrons through heat of up to 2500 Celsius.
- The Lanthanum Hexaboride emits a brighter beam.
- The Field Emission Gun (FEG) provides the brightest beam with the highest resolution but also requires an extremely high vacuum.

Back-Scatter Electron (BSE) is one of the setting used in the SEM during this study which is used to differentiate electron reflections in the analyzed material to depict what mineral exist in the sample using the mean atomic number of the mineral, where heavier elements appear brighter in resulting image (Ali et al., 2023). Energy dispersive X-ray (EDX) is the additional setting used in analyzing the chemical composition of marked areas within a sample (Ali et al., 2023).

4 Results

4.1 Result summary

Eleven samples from inferred density flow deposits of the Orbuklukeli section were studied. Lithoclast is the dominant frame component in researching density

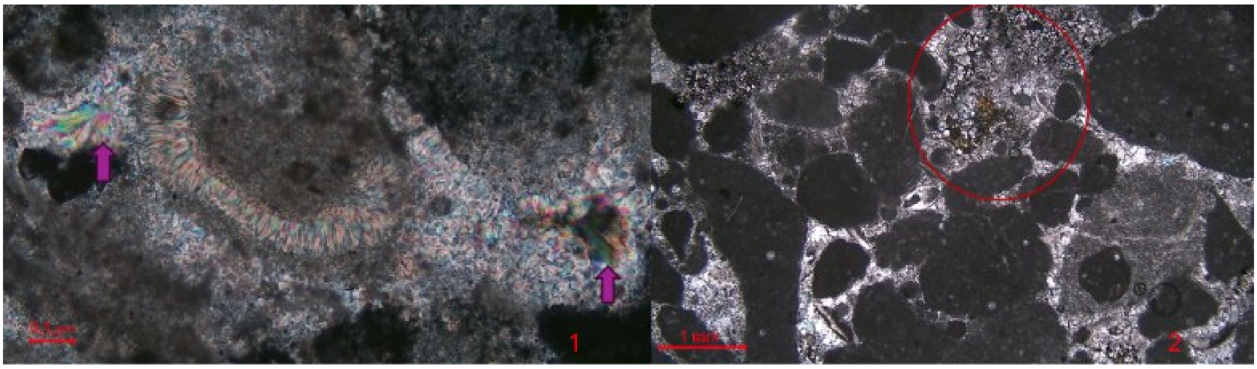

Figure 5. 1. Botryoidal cement highlighted by the pink arrows. 2. Irregular calcite crystals which fills the space between the grains, best represented in the red circle.

flows and is differently abundant in the samples, where DF1, DF3 and DF4 is clast supported and DF2, DF5 and DF6 is matrix supported. The thin-sections studied show different classifications within the density flows which are grainstone, calci-mudstone, floatstone and rudstone, while wackestone and packstone occur within lithoclasts. There are three different types of cement in the samples.

Botryoidal cement depicted in figure 5.1. is a radial fibrous structure of cement that is intergranular. It is irregular calcite crystals that fills the space between the grains which is depicted in figure 5. 2. Microspar is a fine cement which originates from recrystallisation from micrite (Flügel, 2010). The microspar is an intergranular cement.

Glauconite with its chemical composition $(K,Na)(Fe^{3+},Al,Mg)_2(Si,Al)_4O_{10}(OH)_2$ is the green to yellow grains within some of the samples that creates films and coatings on or around the grains. Glauconite forms under a slow sedimentation rate and slightly depleted oxygen because of high organic matter decomposition through pores in the host material. Glauconite replaces the substrate gradually which is normally mineral fragments such as feldspar and quartz, foraminifera or microfossil or biogenic carbonate debris (Odin & Matter, 1981). Glauconite is optimally created in the ocean between a depth of 60 – 500 m, but can also form at shallower depths (Odin & Matter, 1981).

The samples have been organized in density flow sections from DF1 – DF6 as depicted in the log in figure 6. DF1 includes OR25, OR26, OR27, OR28 and OR29. DF2 includes OR35 and OR36. DF3 includes OR50. DF4 includes OR59. DF5 includes OR72. DF6 includes OR76.

4.1.1 Density flow 1 (DF1)

DF1 consists of several horizontal beds. The lowermost bed consists of a 9 cm thick red quartz-rich microconglomerate with associated spotted glauconite grains. There are both limestone clasts and microcrystalline quartz clasts within a sparitic and botryoidal cement. The base of the bed is beige and highly porous in contrast to the rest of the bed. Above, the second bed consists of a 20 cm thick brownish red quartz-rich microconglomerate. There are both limestone clasts and microcrystalline quartz clasts within a sparitic and botryoidal cement. This bed has a noticeably higher quartz content than the bed below. On top, the third bed consists of a 5 cm pinkish gray microconglomerate with associated spotted glauconite grains. The third bed has clearly less quartz content than the beds below. The fourth uppermost bed consists of a dark brown 3 cm thick microconglomerate with associated spotty glauconite grains. The samples OR25, OR26, OR27, OR28 and OR29 derives from these four amalgamated beds which is displayed in figure 3.

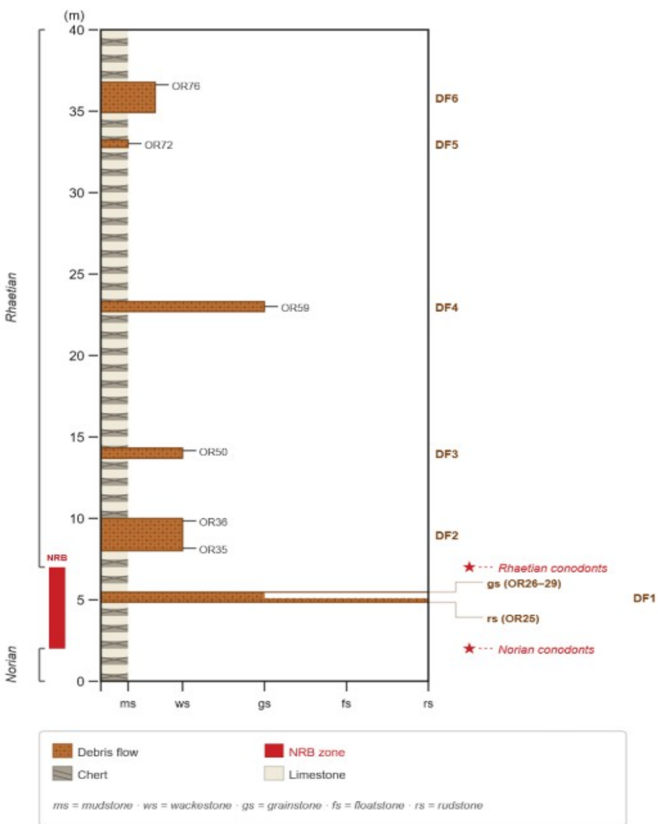

Figure 6. A simplified sedimentary log of the Orbuklukeli section which depicts the density flows (DF1-DF6), the NRB zone, chert/ limestone alteration and carbonate microfacies following Dunham (1962) (Flügel, 2010).

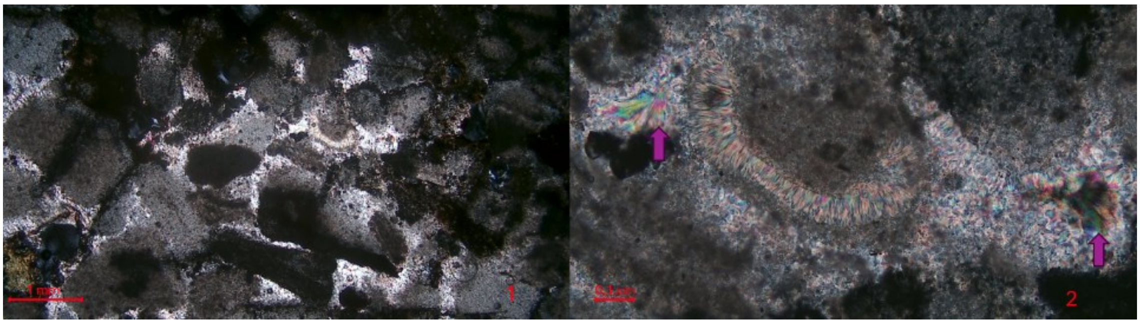

Figure 7. Sample OR25 observed in microscope. 1: Broader view over sample. 2: View of botryoidal cement which is highlighted by the pink arrows.

OR25 is a rudstone with a microsparite as main cement (figure 7.1). Botryoidal cement occurs within the sample as shown in figure 7.2. Lithoclasts contains mainly microcrystalline quartz but does also have carbonate lithoclasts. The carbonate lithoclasts are classified as calci-mudstone. No bioclasts could be certainly identified in OR25, while there still is broken bioclasts in the sample. No glauconite is observed in this sample.

mudstone (figure 8.2). Calci-mudstone lithoclasts are dominating the sample. The bioclasts include disarticulated bivalves and gastropods. The green algae (Dasycladales) occur with a size of 0,3 mm; the fossil is partly biodegraded and is identified for its rounded structure, radial lateral pores and a void at the centre (figure 8.3). Ostracods and brachiopods could exist but were too biodegraded to identify with certainty. Glauconite occurs as coatings and filaments between and within the clasts.

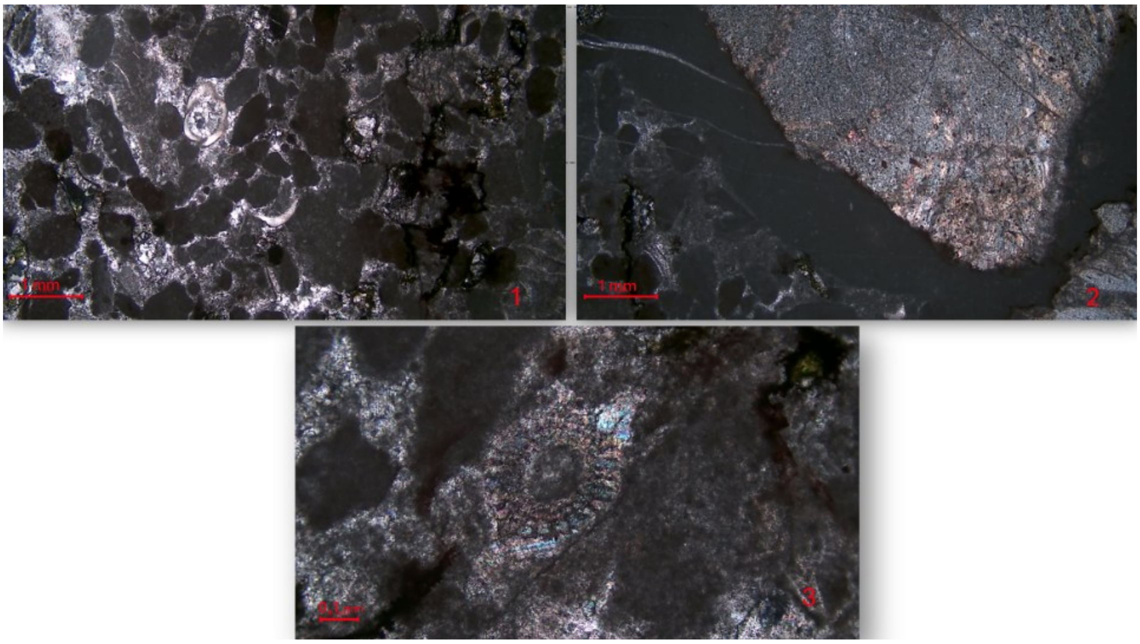

Figure 8. sample OR26 observed in microscope. 1: Broader view of the sample. 2: Lithoclast of microcrystalline quartz inside an lithoclast of calci-mudstone (Flügel, 2010). 3: Green algae (Dasycladales).

OR26 is a grainstone with lithoclasts (figure 8.1). A microcrystalline quartz lithoclast occurs within a lithoclast of calci-

SEM-analysis of OR26 shows microcrystalline quartz within the mudstone lithoclast (figure 9).

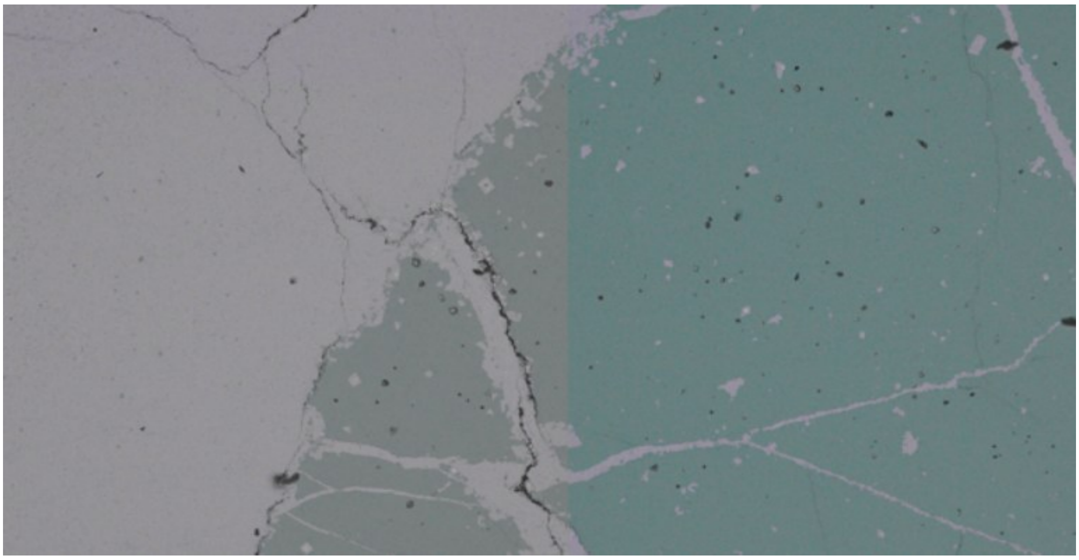

Figure 9. Backscatter SEM image showing a quartz grain within the carbonate lithoclast, which is displayed in figure 8.2. Blue colour is the microcrystalline quartz and white is calcite.

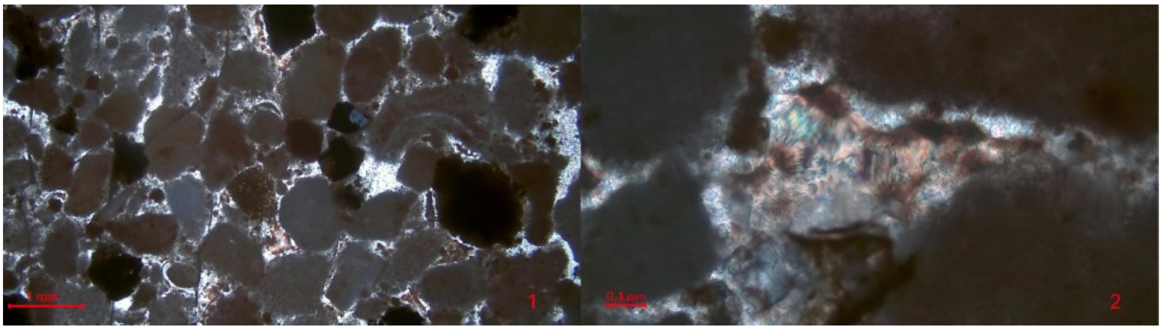

Figure 10. 1: Broader view of sample OR27. 2: Botryoidal cement between grains.

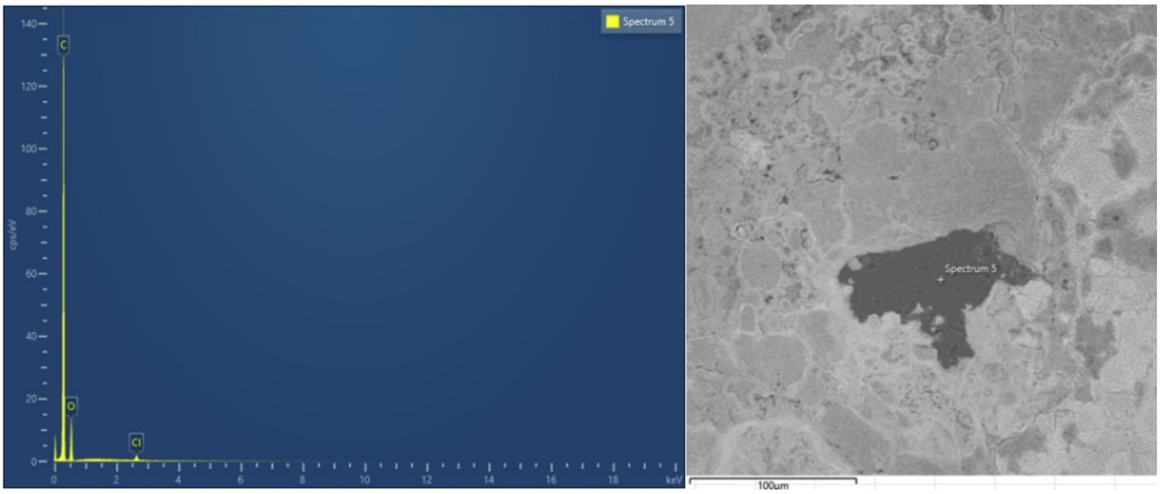

Figure 11. SEM-analysis over spectrum 5 which is marked on the right picture and a chart of the elemental composition.

OR27 is a grainstone dominated by microcrystalline quartz lithoclasts and botryoidal cement (figure 10). Microspar cement occurs in a smaller amount. Disarticulated bivalves occur within the sample. Ostracods and brachiopods could occur but couldn’t be identified with certainty because of biodegradation. No glauconite was observed within the sample.

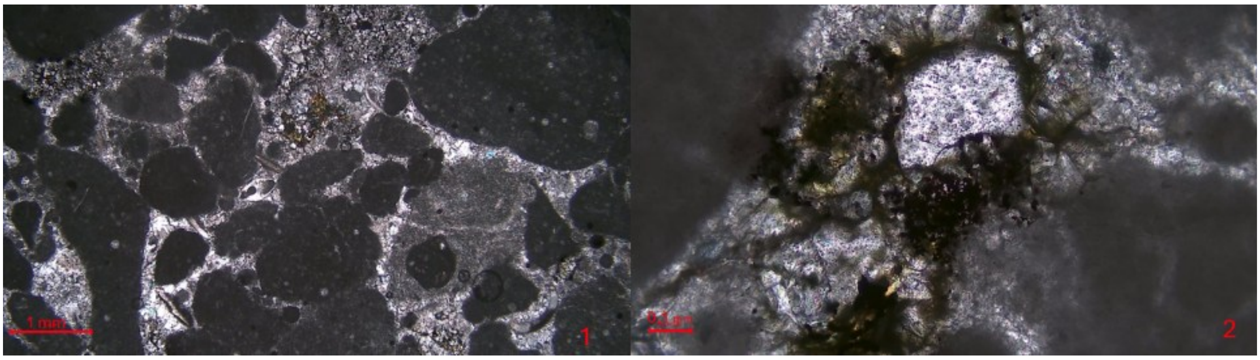

Figure 12. Microscope view of sample OR28. 1: Broader view over the sample. 2: glauconite observed creating coatings and filaments around a grain.

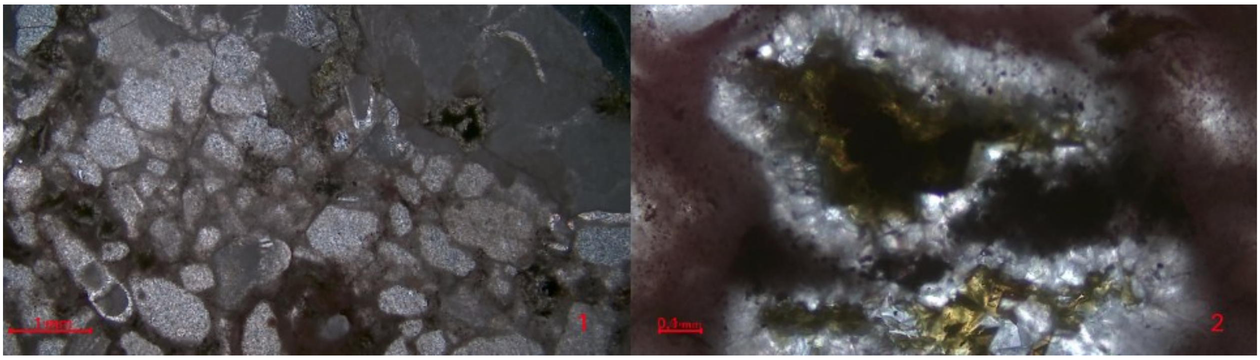

Figure 13. Microscope view of sample OR29. 1: Broader view of the sample. 2: Glauconite within the matrix.

SEM-analysis of OR27 highlighted the presence of organic matter (figure 11).

OR28 is a grainstone with blocky/mosaic cement and a small amount of botryoidal cement which fills the intergranular space (figure 12.1).
The lithoclasts composition is carbonate. The lithoclasts have a high chance of including bivalves but could not be identified with certainty. Glauconite creates coatings and filament between and on the grains which is depicted in figure 12.2.

OR29 is a grainstone with rounded microcrystalline lithoclasts (figure 13.1). The lithoclasts are more rounded compared to the other grainstone samples in DF1. Micritized bioclasts occur within the sample. The bioclasts identified was bivalves and gastropods. Glauconite was identified and creates coatings and filaments in and between the grains (figure 13.2).

4.1.2 Density flow 2 (DF2)

DF2 is a Orthoconglomerate (gravel sized, clasts supported) with limestone clasts in a calcimudstone matrix. Gray in colour. No bedding, and without any clear way-up structure. Clast size varies from granule to cobble. 2m thick.

At the base of density flow 2, sample OR35 represents the calci-mudstone matrix from the deposit which contains both disarticulted bivalves and gastropods (figure 14.2). Micritized bioclasts occurs within the sample (figure 14.1). Calci-spheres are

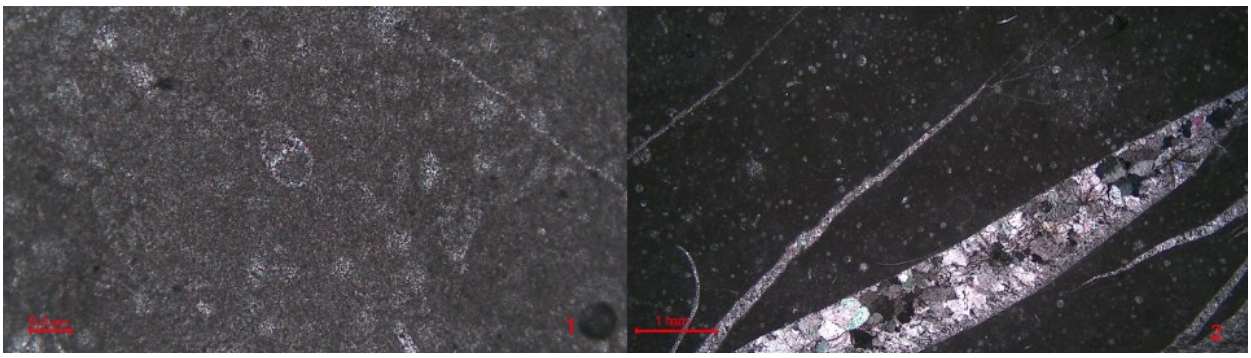

Figure 14. Microscope view of sample OR35. 1: micritized bioclast. 2: broader view of calcite veins and calcispheres within the sample.

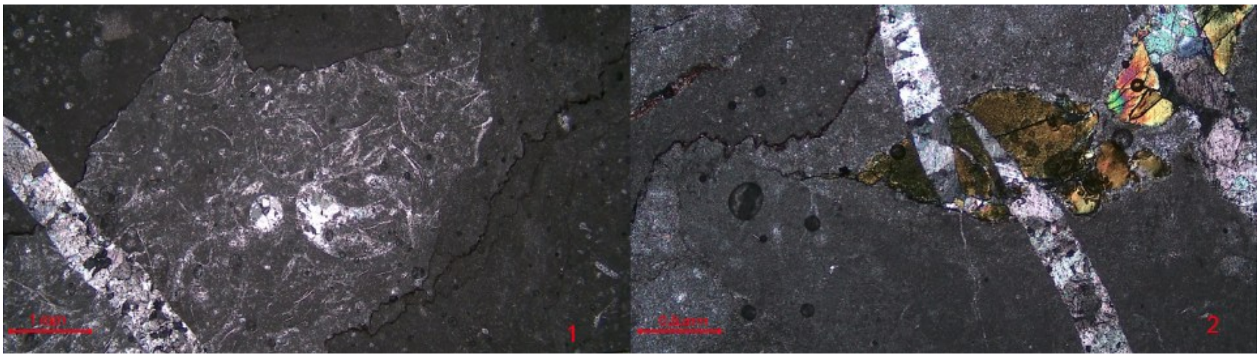

Figure 15. Micropscope view of sample OR36. 1: lithoclast filled with bivalve filaments. 2: glauconite and stylolites.

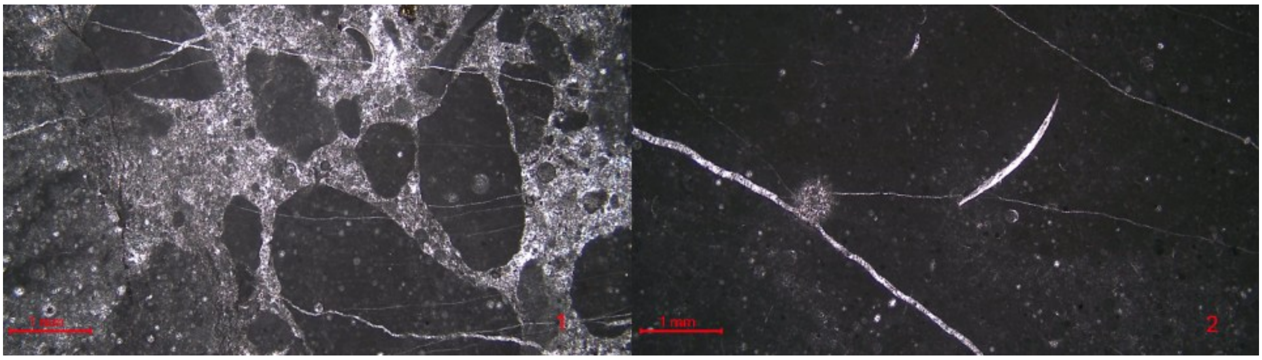

Figure 16. Microscope view of sample OR50. 1: broader view of the sample. 2: bivalve bioclast, calcispheres and a micritized bioclast.

frequent. Ostracods and brachiopods could exist within the sample but could not be identified with certainty. No glauconite was observed in the sample.

At the top of density flow 2, sample OR36 represent a floatstone with calci-mudstone matrix and lithoclasts classified as packstone (figure 15.1). The intraclasts are filled with bioclasts and their margins are not sharped but are identified for their density of bioclasts (figure 15.1). Borders can also be surrounded with stylolite. Lithoclastic packstone are filled with bivalve filament (figure 15.1). The bioclasts include disarticulated bivalves and gastropods within both the matrix and packstone. Micritized bioclasts occur within the sample. Ostracods and brachiopods could occur, but identification couldn't be made with certainty. Glauconite creates coatings and filaments in and between the grains.

4.1.3 Density flow 3 (DF3)

DF3 is a Orthoconglomerate (gravel sized, clasts supported) with limestone clasts in a calci-mudstone matrix. Gray in colour. In one horizontal bed without internal bedding. Clast size mostly pebbles and varies less than in DF2. Roughly 30 cm thick.

At the top of Density flow 3, sample OR50 represent a rudstone dominated by lithoclasts with a calci-mudstone matrix (figure 16.1 – 16.2). Microspar cements occur as intergranular fills. The bioclasts within the sample are disarticulated bivalves, some micritized, and gastropods (figure 16.2). Calci-spheres occurs (figure 16.2). Ostracods and brachiopods could exist but couldn't be identified with certainty. The occurrence of oxidized iron could suggest the possibility of glauconite existing within DF3.

4.1.4 Density flow 4 (DF4)

DF4 is a 30 cm conglomeratic limestone with three internal horizontal beds. Bottom bed consists of a 9 cm beige microconglomerate. On top is a beige 11 cm microconglomerate with a conglomerate base. The conglomerate base has pebble and cobble sized clasts going up into the microconglomerate. The uppermost internal bed is a beige and gray 10 cm orthoconglomerate of cobble and pebble sized clasts.

At the middle of density flow 4,

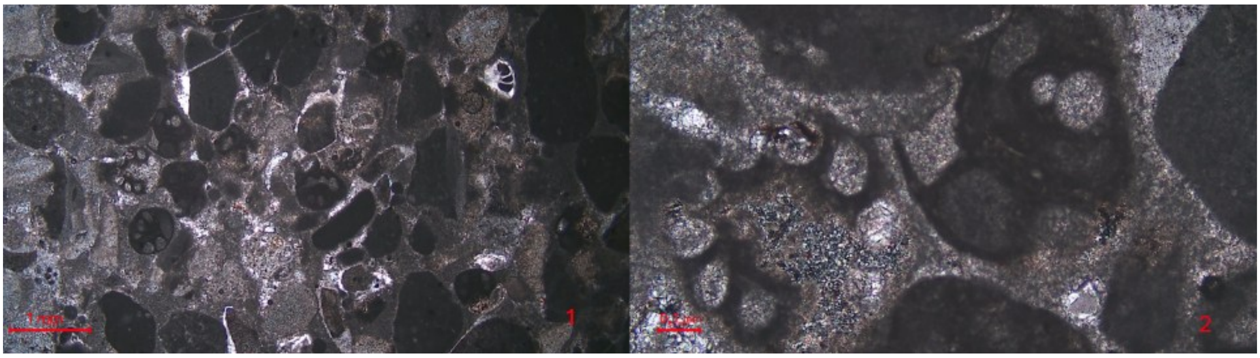

Figure 17. Microscope view of sample OR59. 1: broader view of the sample. 2: Tubiphytes shown within the matrix.

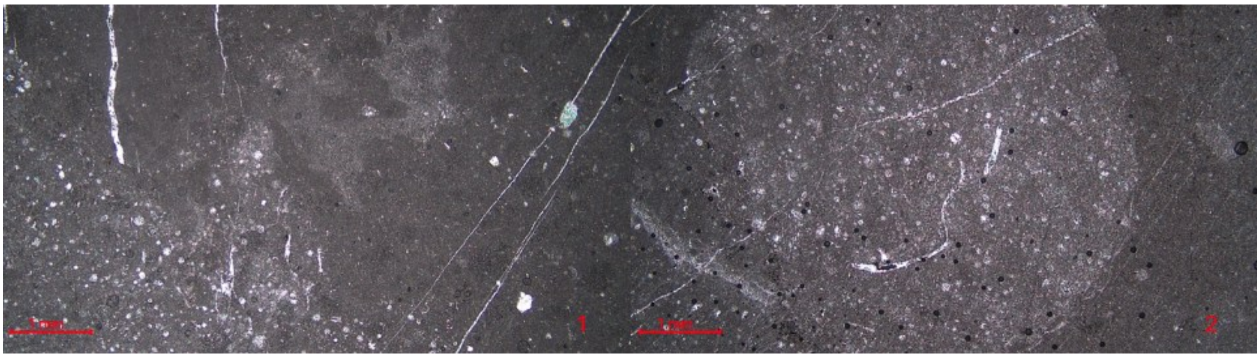

Figure 18. Microscope view of sample OR72. 1: Broader view of sample and the border between matrix and intraclast. 2: broader view of sample and the border between intraclast and matrix.

sample OR59 represent a grainstone with microspar ce ment that occur intergranular (figure 17.1). Bioclasts include disarticulated bivalves, micritized bioclasts and gastropods. Crinoidea is also identified and is characterized for its light extinction pattern with rotating polarized light. Tubiphytes is identified in the sample with a size of between 0.1 – 0.5 mm and creates the dominant group of grains within the grainstone (figure 17.1 – 17.2). Ostracods and brachiopods could exist within the sample but could not be identified with certainty. No glauconite was observed.

4.1.5 Density flow 5 (DF5)

DF5 consist of a 50 cm thick bed of beige-colored limestone. Due to lacking field observation no further detailed description can be made.

At the middle of density flow 5, sample OR72 represent a floatstone with calci-mudstone matrix and with lithoclasts of wackestone. The intraclasts is filled with bioclasts and the border between lithoclasts and the surrounding calci-mudstone is not sharp but highlighted by the amount of bioclasts in an area (figure 18.1 – 18.2). Stylolites occur and create a border between lithoclasts and the surrounding calci-mudstone. Bioclasts that occur within both the wackestone and calci-mudstone

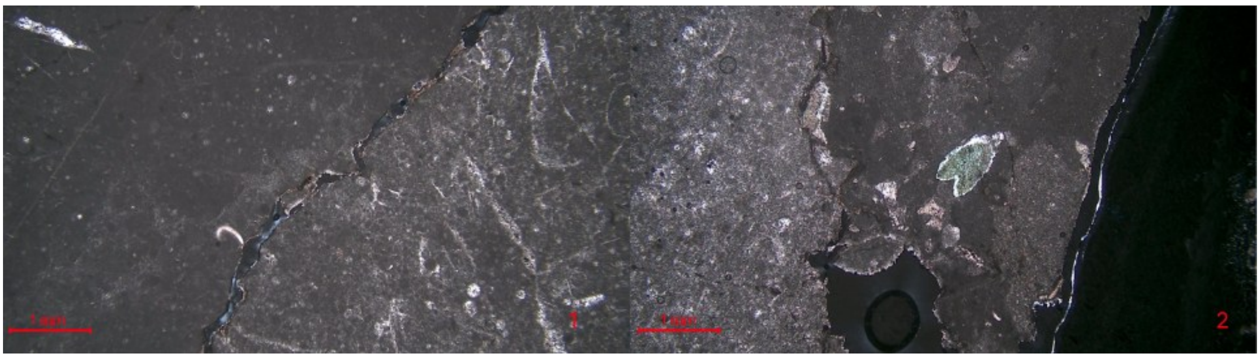

Figure 19. Microscope view of sample OR76. 1: broader view of the sample. 2: a green Crinoidea within the matrix.

matrix are disarticulated bivalves, micritized bioclasts and gastropods. Calci-spheres occur within the sample. Ostracods and brachiopods could occur but could not be identified with certainty. No glauconite was observed.

4.1.6 Density flow 6 (DF6)

DF6 is a Orthoconglomerate (gravel sized, clasts supported) with limestone clasts in a calci-mudstone matrix. Gray in colour. No bedding, and without any clear way-up structure. Clast size varies from granule to cobble. Roughly 2 m thick.

At the top of density flow 6, sample OR76 represent a floatstone consisting of wackestone lithoclasts in a calci-mudstone matrix (figure 19.1). The lithoclasts is filled with bioclasts and the border between lithoclast and surrounding calci-mudstone is hard to depict but is identified by its density of bioclast in an area as well as stylolite's which creates borders between the calci-mudstone and wackestone (figure 19.1). Bioclast include disarticulated bivalves, micritized bioclasts and crinoids in both the lithoclasts and matrix (figure 19.2). Calci-spheres occur within the sample. Ostracods and brachiopods could occur within the sample but couldn't be identified with certainty. No glauconite was observed.

5 Discussion

5.1 Density flow 1

Four out of the five samples from DF1 are classified as grainstone, indicating a depositional environment with high energy. OR25 which is the lower most sample of DF1 is classified as rudstone. Rudstone indicates formation through erosion and transport which could be an indicator for slope environment. DF1 indicates mostly a high energy source environment which is different from the other density flow sections which has calci-mudstone lithoclasts.

While the lithoclasts have a lot of microcrystalline quartz, they predominantly consist of calci-mudstone and differ in structure and roundness between the samples in DF1. OR29 has rounded lithoclasts which indicate a longer transport compared to the other samples.

OR26 has a lithoclast within a lithoclast which indicate two different depositional episodes. While the inner lithoclast is microcrystalline quartz, the surrounding lithoclast has a carbonate composition, which indicates that the source region was different. Almost all other lithoclasts except for OR27 where approximately half lithoclasts consist of microcrystalline quartz, are made of calci-mudstone which indicate a low energy source region but cannot be specified with only lithoclast composition. With indicators like dasycladales and botryoidal cement, the source environment could be shallow to intermediate platform origin (Flügel, 2010).
There is large size difference between the grains in all DF1 which indicate a fast deposition with poor sorting.
Following interpretations based on Flügel (2010), Dasycladales in OR26 is an indication for a photic zone as the Dasycladales rarely exist outside the lagoon or carbonate barrier area. The disarticulated bivalve shells indicate transport that separate the shell halves.
The micritization of bioclasts indicates exposure on the sea floor where m icroorganisms bored into the grain surface before the final deposition of the density flow.

The botryoidal cement that is found in OR25, OR27 and OR28, indicates early marine cement that forms at slopes in a marine phreatic environment (cf. Flügel 2010). While the botryoidal cement occurs as a second-generation cement filling the centre part of the void between the grains, post-dating an earlier cement generation on the grain surface (figure 5.1), it is still interpreted as an early marine cement. Botryoidal cements are known during the Triassic in reef slope deposits.

Glauconite occurs in OR26, OR28 and OR29. Glauconite normally forms at a depth of 60-500 m in the outer portions of the continental shelf, where sedimentation rate is slow. This suggests that the sediment accumulated in this environment before it was re-deposited (Odin & Matter, 1981).

The material of DF1 has an origin from different depths which indicates that DF1 have relocated and transported material from different environment at different sections of the continental slope. Seismic activity could be the trigger for this density flow considering the seismic activity already regionally known during the late Norian (Tekin et al., 2020). The lithoclasts of microcrystalline quartz with rounded grains and associated glauconite indicates transport through a river and river delta. The transported material was probably deposited in a high energy environment that is shallow considering occurrence of Dasycladales and the botryoidal cement. The presence of transported glauconite and of lower energy calci-mudstone as lithoclast indicate an intermediate redeposition at a depth of between 60 – 500 m (Odin & Matter, 1981), with low sedimentation rate before continuing the transport. Density flow has then transported this lithified part down the slope, (Odin & Matter, 1981) until it got deposited at bathyal depth. (Tekin et al., 2020).

An alternate interpretation is that the density flows are the reminiscence of seamount with a hydrothermal system which collapsed. Botryoidal cement, organic matter identified in the SEM-analysis of OR26 (which in this case could be hydrocarbons) and glauconite are all consistent with a hydrocarbon seep environment. The seamount was shallow enough to bear dasycladacean. This elevated seep then collapsed creating the density flow seen here. While this alternative interpretation is an event that could likely have happened, we would need further geochemical analysis to confirm or give it more room for discussion.

5.2 Density flow 2

DF2 samples was classified as floatstone with a calci-mudstone matrix which is an indicator for low energy environment. DF2 lithoclasts were both classifi cations as packstone and wackestone which indicates th at the lithoclasts source area were of a higher energy environment.

The lithoclasts in DF2 has filaments of disarticulated bivalves which indicates that it has been a high energy environment which then deposited in a place where the bivalves could gather to create a packstone lithoclasts. There exists stylolite bet ween the lithoclasts and the matrix which indicates pressure solution after the deposition which means the lithoclasts is older than the surrounding calci-mudstone (Flügel, 2010).

The bivalves in both samples were disarticulated which indicate that they have been transported as halves. The filament bivalves depict a pelagic to hemipelagic environment which indicates a deeper environment instead of shallow and is typical for the Triassic period (Flügel, 2010). Calcispheres which was found in DF2 indicate slope environment during the late Triassic (Flügel, 2010). Micritized bioclasts indicate that the bioclasts was exposed on the ocean floor where microboring organisms could "attack" the grain surfaces before it was later buried (Flügel, 2010).

Glauconite only occur in OR36 which indicates that the lithoclasts in OR36 could have incorporated glauconite-bearing material with it before depositing in the bathyal zone. It also indicate that the lithoclasts could come from a depth of 60 – 500m (Odin & Matter, 1981).

Compared to DF1 the environment was probably not as shallow because of the low energy indicators. The calcispheres and bivalve filament lithoclasts allow the interpretation of a slope environment at the outer shelf. Stylolites confirm that there was burial and diagenesis. The trigger for the density flow could still be seismic activity but is not as likely compared to DF1 which was closer to the late Norian shown in figure 6. which seismic activity is already known (Tekin et al., 2020).

5.3 Density flow 3

OR50 is classified as a rudstone with calci-mudstone matrix which is a combination where finer matrix and clasts occur together. The rudstone component means it has been through erosion and transport. The wackestone matrix together with the bigger lithoclasts indicate a deposition typical for density flows. The lithoclasts is the main component in DF3.

The lithoclasts dominate the sample compared to DF1 and DF2. The lithoclasts are composed of mainly calci-mudstone. Lithoclast size varies a lot and indicate poor sorting and indicates fast deposition.

With the help of Flügel (2010),the interpretation of the disarticulated bivalves indicate transportation which seperated the halves of the bivalve. There were also micritized bioclasts which indicate exposure for microboring organismns to "bore" the bioclasts on the ocean floor. Calcispheres was also identified which indicate a slope enviornment during the late Triassic.

OR50 have microspar cement which indicated diagenetic alteration after burial (Flügel, 2010). Compared to DF1 which had botryoidal cement, the microspar cement characterizes a different diagenetic situation.

There is a possibility that glauconite occurs because of "rust" holes in OR50 which indicates that the depth of 60-500m is possible for the depth of the origin source rock of the lithoclasts (Odin & Matter, 1981).

The environment which the calcispheres and glauconite indicate that DF3 probably come from the outer shelf on the slope. The high amount of lithoclasts depict a high-intensity density flow event.

5.4 Density flow 4

OR59 is a grainstone which indicated high energy environment. DF4 resemble DF1 in how high the energy was because of the lack of mud.

Following Flügel (2010), the interpretation of OR59 suggests the presence of tubiphytes that may reflect different depositional environments. Some tubip hytes are indicative of mid-ramp settings, whereas others are associated with low-energy, low-oxygen conditions. This suggests that the tubiphytes in OR59 likely represent either a mid-ramp or an outer-ramp environment. Crinoids were also found in DF4 which indicates slope environments during the late Triassic. There are also disarticulated bivalves which gives indications of transport and micritized bivalves which indicates exposure to microboring organisms on the ocean floor in a low energy environment.

Microspar cement which indicate diagenetic alteration after burial (Flügel, 2010).

Tubiphytes and crinoids are indicators for a slope environment (Flügel, 2010). DF4 could originate from the upper slope instead of shallow water. The grainstone texture indicates a high energy deposition.

5.5 Density flow 5

OR72 a floatstone, with a calci-mudstone matrix and wackestone lithoclasts. Wackesto ne lithoclasts are less than 10% grains which indicates a lower energy environment than in the preceding density flows.

The lithoclasts is a wackestone filled with bioclasts with borders to the calci-mudsone that are hard to depict. Stylolites creates borders between lithoclasts and matrix which depict diagenetic alteration after burial (Flügel, 2010).

Following Flügel (2010) interpretations of bioclasts, the disarticulated bivalves indicate transport. The bivalve shells have been micritized which means they have been exposed to microboring organisms at the sea floor before burial. Crinoids was found which indicate slope environment during the late Triassic. Calcispheres in OR72 indicate that slope/deeper shelf environments and is a bathymetric indicator for shelf ledge and slope environments.

The stylolites that were found at the boundary of the lithoclasts indicate that the lithoclasts is older than the calci-mudstone and indicate that there was diagenesis after the burial of the density flow.

The conjunction of crinoids, calcispheres and calci-mudstone matrix indicate that it was a deeper environment with less energy and can be interpreted as slope or outer shelf environment. The wackestone lithoclasts incorporate d in the calci-mudstone matrix indicates mixing of material at deep sea levels along the slope. Stylolite confirm that burial with diagenesis occurred after the events mentioned before.

5.6 Density flow 6

OR76 is classified as a floatstone with peloidal wackestone lithoclasts in a calci-mudstone matrix, indicates that it has been a low energy environment. The peloids is indicators for low energy environments with platform carbonates as shallow tidal or subtidal, peloids could also occur at slope environments. The wackestone could also indicate a low-energy depositional phase.

The lithoclasts observed in OR76 is similar in situation as DF5, as the borders of lithoclasts and calci-mudstone is hard to depict but is depicted by the amount of bioclasts. This could indicate the same origin material as DF5. Stylolites are dissolution horizons that develop during late diagenesis after lithification.

Following Flügel (2010) interpretations of bioclasts, the disarticulated bivalves indicates transport. The micritized bivalves indicates that there were exposed at the ocean floor to microborring organisms before burial. Crinoids in OR76 indicate slope environments during the late Triassic period. Calcispheres occur within the sample which indicate deeper shelf to slope environments during the Mesozoic peroid.

Following the crinoids and calcispheres interpretations it strongly indicates that the origin of DF6 is from outer shelf to slope environment while the peloids indicate that there has been either mixing of more shallow material or diagenetic alteration.

6 Conclusion

In this study, eleven rock samples were petrographically analysed with the purpose of interpreting the source and depositional environment for six density flow deposits from the Orbuklukeli section in southern Turkey.

Density flow 1 include carbonate constituents of a shallow water environment (Dasycladales, botryoidal cement), with inclusions of glauconite, which could either indicate an inner- to outer shelf environment or transport of glauconite through deltas.

Density flow 2 shows indicators of slope to outer shelf environment which is interpreted from the bivalve filaments and calcispheres within the lithoclasts. The floatstone with calci-mudstone matrix indicate low-energy depositional environment.

Density flow 3 is interpreted to have its origin from outer shelf to slope environment because of the calcispheres and possible glauconite. The high amount of lithoclasts indicate an intensive density flow event.

Density flow 4 depicts indicators of upper slope environment which tubiphytes and Crinoidea indicates. The grainstone indicate a high energy deposition.

Density flow 5 and 6 have similar features indicating a floatstone classification with wackestone-lithoclasts, crinoids and calcispheres. This is consistent with Triassic slope to outer shelf environment. These similar indicators give the interpretation that they originate from similar environments.

Conclusively, the density flows follow a trend of initially being transported from shallow-marine environments (DF1) and later from deeper environments (DF2-DF6). Further geochemical analysis would be needed for the competing interpretation of DF1 about the hydrothermal seamount-collapse to better understand what really took place.

7 Acknowlagements

I want to thank my supervisors Sylvain Richoz and Niklas Gunnarsson. Without my supervisors guidance i would not have made this work as efficient and proficient as it has been, especially the thin-sectioning part.

8 Refrences

Ali, A., Zhang, N., & Santos, R. M. (2023). Mineral Characterization Using Scanning Electron Microscopy (SEM): A Review of the Fundamentals, Advancements, and Research Directions. Applied Sciences, 13(23). https://doi.org/10.3390/app132312600

Flügel, E. (2010). Microfacies of Carbonate Rocks Analysis, Interpretation and Application (Vol. Second Edition). Springer-Verlag Berlin Heidelberg https://doi.org/10.1007/10.1007/978-3-642-03796-2

Galbrun, B., Boulila, S., Krystyn, L., Richoz, S., Gardin, S., Bartolini, A., & Maslo, M. (2020). "Short" or "long" Rhaetian ? Astronomical calibration of Austrian key sections. Global and Planetary Change, 192. https://doi.org/10.1016/j.gloplacha.2020.103253

Kovács, Z., Demangel, I., Baldermann, A., Hippler, D., Schmitt, A. D., Gangloff, S., Krystyn, L., & Richoz, S. (2022). The Calcium Isotope (δ44/40Ca) Record Through Environmental Changes: Insights From the Late Triassic. Geochemistry, Geophysics, Geosystems, 23 (12). https://doi.org/10.1029/2022gc010405

Kovács, Z., Demangel, I., Richoz, S., Hippler, D., Baldermann, A., & Krystyn, L. (2020). New constraints on the evolution of 87Sr/86Sr of seawater during the Upper Triassic. Global and Planetary Change, 192. https://doi.org/10.1016/j.gloplacha.2020.103255

Maron, M., Rigo, M., Bertinelli, A., Katz, M. E., Godfrey, L., Zaffani, M., & Muttoni, G. (2015). Magnetostratigraphy, biostratigraphy, and chemostratigraphy of the Pignola-Abriola section: New constraints for the Norian-Rhaetian boundary. Geological Society of America Bulletin. https://doi.org/10.1130/b31106.1

Mulder, T., & Alexander, J. (2001). The physical character of subaqueous sedimentary density flows and their deposits. Sedimentology, 48 (2), 269–299. https://doi.org/10.1046/j.1365-3091.2001.00360.x

Odin, G. S., & Matter, A. (1981). De glauconiarum origine. Sedimentology, 28(5), 611–641. https://doi.org/10.1111/j.1365-3091.1981.tb01925.x

Ogg, J. G., Chen, Z. Q., Orchard, M. J., & Jiang, H. S. (2020). The Triassic Period. In Geologic

Time Scale 2020 (pp. 903–953). https://doi.org/10.1016/b978-0-12-824360-2.00025-5

Parlak, O., & Robertson, A. (2004). The ophiolite-related Mersin Melange, southern Turkey: its role in the tectonic–sedimentary setting of Tethys in the Eastern Mediterranean region. Geological Magazine, 141(3), 257–286. https://doi.org/10.1017/s0016756804009094

Preto, N., Kustatscher, E., & Wignall, P. B. (2010). Triassic climates — State of the art and perspectives. Palaeogeography, Palaeoclimatology, Palaeoecology, 290(1-4), 1–10. https://doi.org/10.1016/j.palaeo.2010.03.015

Reijmer, J. J. G., Palmieri, P., & Groen, R. (2012). Compositional variations in calciturbidites and calcidebrites in response to sea-level fluctuations (Exuma Sound, Bahamas). Facies, 58(4), 493–507. https://doi.org/10.1007/s10347-011-0291-z

Rigo, M., Jin, X., Godfrey, L., Katz, M. E., Sato, H., Tomimatsu, Y., Zaffani, M., Maron, M., Satolli, S., Concheri, G., Cardinali, A., Wu, Q., Du, Y., Lei, J. Z. X., van Wieren, C. S., Tackett, L. S., Campbell, H., Bertinelli, A., & Onoue, T. (2024). Unveiling a new oceanic anoxic event at the Norian/Rhaetian boundary (Late Triassic). Sci Rep, 14(1), 15574. https://doi.org/10.1038/s41598-024-66343-z

Rigo, M., Onoue, T., Tanner, L. H., Lucas, S. G., Godfrey, L., Katz, M. E., Zaffani, M., Grice, K., Cesar, J., Yamashita, D., Maron, M., Tackett, L. S., Campbell, H., Tateo, F., Concheri, G., Agnini, C., Chiari, M., & Bertinelli, A. (2020). The Late Triassic Extinction at the Norian/Rhaetian boundary: Biotic evidence and geochemical signature. Earth-Science Reviews, 204. https://doi.org/10.1016/j.earscirev.2020.103180

Tekin, U. K., Krystyn, L., Okuyucu, C., Bedi, Y., & Sayit, K. (2020). Late Triassic to Early Jurassic radiolarian, conodont and ammonite assemblages from the Tavuscayiri block, Mersin Mélange, southern Turkey: Time constraints for the T/J boundary and sedimentary evolution of the southern margin of the northern Neotethys. Geodiversitas, 42(27). https://doi.org/10.5252/geodiversitas2020v42a27

Tekin, U. K., Okuyucu, C., Sayit, K., Bedi, Y., Noble, P. J., Krystyn, L., & Göncüoglu, M. C. (2018). Integrated Radiolaria, benthic foraminifera and conodont biochronology of the pelagic Permian blocks/tectonic slices and geochemistry of associated volcanic rocks from the Mersin Mélange, southern Turkey: Implications for the Permian evolution of the northern Neotethys. Island Arc, 28(2). https://doi.org/10.1111/iar.12286

Tidigare skrifter i serien "Examensarbeten i Geologi vid Lunds universitet":

684. Olsson Roso, Céline, 2024: Fåglarnas ursprung och tidiga utveckling. (15 hp)
685. Nawrocki, Bartosz, 2024: Karaktärisering av Cr-spinell i den ordoviciska Loka-formationen vid Skultorps stenbrott, Billingen. (15 hp)
686. Rydh, Alexander, 2024: Unraveling Magnetic Anomalies: A Study of Earth's Field Asymmetries during the Laschamps Excursion. (15 hp)
687. Svensson, Ludvig, 2024: Echoes of impact: A petrographic analysis and classification of impact breccias from Hummeln, Sweden. (15 hp)
688. Pålsson, Malin, 2024: Detektion av utsläppsplymer med avancerat ekolod – Undersökning av utsläpp av avloppsvatten från pappersbruk i havet med EK80, CTD & filmmaterial. (15hp)
689. Ivanovic, Edwin, 2024: Går det att se echinodermernas utveckling och diversifiering under ordovicium i tunnslip? (15 hp)
690. Blomvall, Marlene, 2024: Analys av morfologi, beteende och tafonomi hos ett exceptionellt bevarat fågelfossil från Furformationen (eocen), Danmark . (15 hp)
691. Elfström, Dari, 2024; Geomorfologisk studie av Jezerokraterns kant (Mars): Potentiella mekanismer bakom kraterkantens nuvarande utseende. (15 hp)
692. Andersson, Jacob, 2024: The Cerithium limestone Member at Stevns Klint reflecting the carbonate production recovery after the K/Pg mass-extinction. (45 hp)
693. Adler, Linus, 2024: Petrografisk pilotstudie av en högmetamorf epidotrik bergart från Harbak, västra gnejsregionen i Norge. (15 hp)
694. Fält, Smilla, 2024: Dateringsmetoder för terrestriska nedslagskratrar med fokus på Siljan. (15 hp)
695. Kowal Johnson, Gloria, 2024: Traces of industrialization in a Baltic Sea sediment core with particular emphasis on marine traffic in Bornholmsgattet. (15 hp)
696. Riad, Musa, 2024: Bergkross som filtermedium i artificiell infiltration. (15 hp)
697. Gleisner, Lovisa, 2024: Unravelling primary $\delta^{18}O$ signatures of the 1730-36 Timanfaya parental magmas on Lanzarote. (45 hp)
698. Johansson, Robin, 2024: Instrumentation of multilevel systems with transducers to characterize hydrogeological conditions at a PCE and TCE contaminated site in Helsingborg, Sweden. (45 hp)
699. Neumann, Daniel, 2025: Hydrogeological Dynamics of the Dalköpinge River: Investigating the Dry Spell Anomaly in a Hydrogeological Context. (45 hp)
700. Durdek, Madeleine, 2025: Risk for water shortage in Ystad municipality - An evaluation of aquifer vulnerability to human impact. (45 hp)
701. Bouhal, Farah, 2025: Evolution of calcareous nannoplankton in the Late Triassic: Insights at Eiberg Basin (Austria). (45 hp)
702. Barreby, Linn, 2025: Petrographic Analysis of the Loftarstone Resurge Deposit in the Lockne Impact Structure, Sweden. (45 hp)
703. Dyson, Sarah, 2025: Environmental change in the Late Weichselian on the Kullen Peninsula. (45 hp)
704. Kardakos, Nikolaos, 2025: Caprock and reservoir assessment for CO2 storage in Lower Palaeozoic Formations of the Baltic Sea subsurface: Textural, structural and mineralogical characterization using X-ray Computed Tomography, geochemistry and microscopy. (45 hp)
705. Filbà i Serra, Laura, 2025: Weichselian ice dynamics in Jämtland: Lithostratigraphic study of the Köttsjön till deposits. (45 hp)
706. Bäckehag, Kristoffer, 2025: Petrografisk studie av pseudotachylitisk breccia från nedslagskratern Siljan. (15 hp)
707. Zellman, Oskar, 2025: Karaktärisering av laminerade marina sediment under ett globalt utdöende (silur, Gotland). (15 hp)
708. Jögi, Amanda, 2025: En partiell hjärnskål från Åsens krita och dess koppling till den svenska svanödlefaunan. (15hp)
709. Rasmusson, Isak, 2025: Behovet av geologisk kunskap inom utbildning och samhälle: En översikt av geologiskt innehåll i gymnasiets ämnesplaner, antagningar till svenska högskole- och universitetsutbildningar inom geovetenskap och arbetsmarknadens behov av personer med geologisk kompetens. (15hp)
710. Brede, Anton, 2025: Integrating Geological Models and Geophysics to Estimate Hydraulic Properties - Providing a Foundation for Hydrogeophysics Research. (15 hp)
711. Zimmermann, Moa, 2025: Utdöda organismers diet: Karaktärisering av en vertebratkoprolit från Skånes krittid. (15hp)
712. Popa, Alexandra, 2025: Aqueous alteration in Martian meteorite Northwest Africa 11013: An analysis of its extent and origin. (15 hp)
713. Jónsdóttir, Svava Kristin, 2025: Grounding zone wedges in the Nyköping area,

southeastern Sweden. (45hp)

714. Heim, Emelie, 2025: Den sen- och postglaciala landskapsutvecklingen i Tvååker, Halland. (15 hp)

715. Schiemann, Erik, 2025: Pollen och mikrofossil i en borrkärna från nedslagsstrukturen Hummeln. (15 hp)

716. Blomberg, Hampus, 2025: Vegetationsutvecklingen i Halland och Tvååker: sammanställning av underlag till informationsskyltar vid Naturplats Tvååkers Mosse. (15 hp)

717. Östman, Adrian, 2025: En litteraturstudie om grundvattendata och modeller som möjliga verktyg inom mineralprospektering. (15 hp)

718. Belcher, Carl Nils, 2025: Systematiska felkällor i deklinationsdata från sedimentära borrkärnor. (15 hp)

719. Raas, Valérie, 2025: Cosmogenic Radionuclide Evidence for a Solar Particle Storm at 14,300 BP. (45 hp)

720. Bjarkadóttir, Anna Bríet, 2025: Barometry of Clinopyroxene in Xenoliths from the Anaga Region in Tenerife – Constraints on the Magmatic Plumbing System. (45 hp)

721. Grönberg, Joel, 2025: Kan vulkanismen på Kanarieöarna ha uppkommit till följd av en hetfläck?. (15 hp)

722. Cordes, Beatrix, 2025: A review of the contaminant situation of groundwater aquifers in Europe – A historical retrospective and future outlook. (45 hp)

723. Alkasser, Shefaa, 2025: En litteraturstudie om mantelplymhypotesens eventuella tillkortakommanden utifrån ett kanariskt perspektiv. (15 hp)

724. Grönberg, Joel, 2026: Optically stimulated luminescence in Scania: An investigation into its applicability of determining provenance of coastal deposits. (45 hp)

725. Langkjaer, Henrik, 2026: Esker formation during deglaciation of the Scandinavian Ice Sheet, northeast Skåne and Blekinge, Sweden. (45 hp)

726. Corshammar, Johannes, 2026: Petrologisk -petrografisk studie av ankaramitbergarter på Teneriffa. (15 hp)

727. Sonesson, Ville, 2026: BC-koncentrationer i sjösediment: en jämförelse mellan Kina, Schweiz och Finland. (15 hp)

728. Schönherr, Lara, 2026: Structural and petrographic characterization of the Mien impact structure, Sweden. (45 hp)

729. Meret, Ellison, 2026: Characterization of storm-surge deposits: A multi-proxy approach along the northern Halland coast with implications for organic carbon storage. (45hp)

730. Ólafsdóttir Arnholtz, Edda, 2026: Constraining Weichselian high relative sea-level events in Basissletta, northeastern Spitsbergen. (45 hp)

731. Persson, Frida, 2026: Windows of Mars: Impact Craters Along the Martian Dichotomy as Markers for Planetary Evolution. (15 hp)

732. Frödin, Anna, 2026: Industriella utsläpp till Östersjön - En kartläggning av utsläpp och effekter från pappers- och massaindustrin. (15 hp)

733. Österberg, Agnes, 2026: Från sund till ljung: Falsterbonäsets uppkomst och historisk skogsförekomst på Skanörs ljung. (15 hp)

734. Ründla, Karoliina, 2026: Utveckling av markanvändning och vegetation i Söderåsens Nationalpark från senare delen av jägarstenåldern till nutid. (15 hp)

735. Pålsson, Malin, 2026: A Changing Foraminiferal Landscape in the Öresund: Cataloguing the Potentially Invasive Nonionella sp. T1 and Assessing Deep Learning for Species Identification. (45 hp)

736. Magnell, Ylva, 2026: Intracrustal partial melting of garnet amphibolite from southwestern Sweden - a possible analogue for TTG formation. (15 hp)

737. Lindqvist Lindström, Noah, 2026: Petrographic analysis and palaeoenvironmental reconstruction of density flow deposits in the Orbuklukeli section, Mersin Mélange, Southern Turkey. (15 hp)

LUNDS UNIVERSITET

Institutionen för miljö– och geovetenskap
Lunds universitet
Sölvegatan 12, 223 62 Lund